The use of geologic expression workflows for basin scale reconnaissance: A case study from the Exmouth Subbasin, North Carnarvon Basin, northwestern Australia

N. J. McArdle[1], D. Iacopini[2], M. A. KunleDare[1], and G. S. Paton[1]

Abstract

The focus of this study is to demonstrate how seismic attributes can be used in the interpretation workflow to rapidly obtain a high-resolution view of the geology that is imaged within a seismic data set. To demonstrate the efficacy of seismic attribute analysis to basin scale reconnaissance, we apply a workflow to seismic data sets from the Exmouth Subbasin, northwestern Australia, with the aim of determining the geologic expression of the subsurface. Of specific interest are Barrow Group Jurassic and Cretaceous fluvial and marine sediments, that were faulted during the Jurassic-Cretaceous rifting associated with the breakup of East Gondwana. Regional-scale interpretations are made to develop a tectonostratigraphic context to the investigation. Target-level analyses, focused on features of exploration interest identified using regional reconnaissance, are made to calibrate attribute response and demonstrate the effectiveness of seismic attributes for rapid evaluation of prospectivity in the initial stages of exploration. The main structural episodes are distinguished using dip and azimuth attributes, and faulting is expressed using a combination of edge attributes which are used to create fault trend lineations. We observe three main structural trends: the main northeast–southwest Jurassic-Cretaceous syn-rift primary fault orientation of 48°, a secondary trend of 108°, taken to represent secondary conjugate faulting and a third trend of 100° interpreted as the reactivation of these faults into the postrift sediments. Stratigraphic attributes that respond to amplitude and frequency are used to create reservoir scale geobodies of faulted Macedon turbidites, which in turn are used for detailed tuning sensitivity analysis. The final part of the investigation is of the syn-rift magmatic system responsible for sills and dikes that exploit the normal fault network. These intrusive and extrusive features are important as are potential drilling hazards and can act as baffles to hydrocarbon migration.

Introduction

The use of seismic attributes for reconnaissance of seismic data sets is well established and there is extensive literature on this subject spanning the use of complex attributes to identify thin bed, discontinuity, and bright spots due to hydrocarbon effects (Taner and Sheriff, 1977) to reflector dip and azimuth and coherence to identify structural elements (Dalley et al., 1989; Chopra and Marfurt, 2006 and references therein). Recently, more sophisticated image analyses using crossplotting and blending methods have been applied for reservoir (Chopra and Marfurt, 2010) and fracture characterization purposes (Gao, 2013), and fault and thrust analysis (Dutzer et al., 2010; Iacopini and Butler, 2011). Despite the detailed understanding of these imaging techniques, very few studies showing the great potential of these methods at regional and exploration level have been published.

The workflows employed in this study have been deliberately chosen to demonstrate how, by using seismic attributes, an interpreter can quickly and efficiently achieve a regional understanding of subsurface geologic expression. Furthermore, by using high-resolution imaging techniques, it is easy to go from a regional perspective to focused target-level analyses using the same attributes. This rapid transition from regional to detailed analysis is extremely powerful for prospect generation in the early stages of exploration and it also provides a means of critically evaluating the attributes generated. We show here how using traditional 3D seismic attribute analyses, combined with multiattribute combination and visualization techniques to evaluate the tectonostrati-

[1]ffA, Northpoint, Aberdeen, UK. E-mail: NMcArdle@ffa-geosciences.com; MKunleDare@ffa-geosciences.com; gpaton@ffa-geosciences.com.
[2]University of Aberdeen, Geology and Petroleum Geology, School of Geosciences, Aberdeen, UK. E-mail: d.iacopini@abdn.ac.uk.

Manuscript received by the Editor 29 July 2013; revised manuscript received 25 October 2013; published online 31 January 2014. This paper appears in *Interpretation*, Vol. 2, No. 1 (February 2014); p. SA163–SA177, 8 FIGS., 2 TABLES.
http://dx.doi.org/10.1190/1.1440403.

graphic history of the Exmouth Subbasin, northwestern Australia, it is possible to explore regional-scale geologic features with the primary aim of identifying, understanding, and evaluating sedimentary packages with hydrocarbon-bearing potential. This sedimentary basin lends itself perfectly to this study, due to the wealth of high-quality 3D seismic data available, together with numerous exploration wells to correlate our interpretation with. A basemap showing the location and extents of the three data sets is shown in Figure 1 along with sample arbitrary lines which highlight the variability in data quality throughout the sections. Three overlapping 3D seismic data sets covering a total acreage close to 3500 km^2 have been evaluated; these seismic surveys are named *HCA2000A*, acquired in 2000; Indian, acquired in 2000; and Vincent, acquired in 1998. Although the three data sets have similar quality and interpretability in the shallower sections (after the Late Cretaceous postrift phase), only seismic reflectivity from the Indian 3D survey can be resolved with confidence for detailed interpretation of the deeper Early Cretaceous–Jurassic sections, using the seismic data alone.

Structural and fault expression workflows are implemented, highlighting regional structure and fault networks. In particular, we are able to discern information pertaining to the pre-Cretaceous stress field that induced rifting, fault sealing, and reactivation. Attributes that highlight variations in stratigraphic sequences are used to distinguish different depositional features of interest, image existing reservoirs, identify new potential leads, and improve the play concept model.

Geologic setting and petroleum play

The Exmouth Subbasin is located on the northwestern Australia margin and is part of the Northern Carnarvon Basin. It represents a series of Jurassic en echelon structural depressions and has geologic affinities with the Barrow, Dampier, and Beagle Subbasins representing a failed rift system that developed during the early syn-rift phase of the breakup of the northwestern Australian continental margin (Regional geology of the Northern Carnarvon Basin, Australia 2012, Offshore Petroleum Exploration Acreage release, 2012). As part of the offshore Northern Carnarvon Basin, the Exmouth Subbasin evolved from a prerift sag basin in the late Paleozoic through tectonically active polycyclic extension in the Jurassic to Early Cretaceous, producing syn-rift subbasins (with dominant

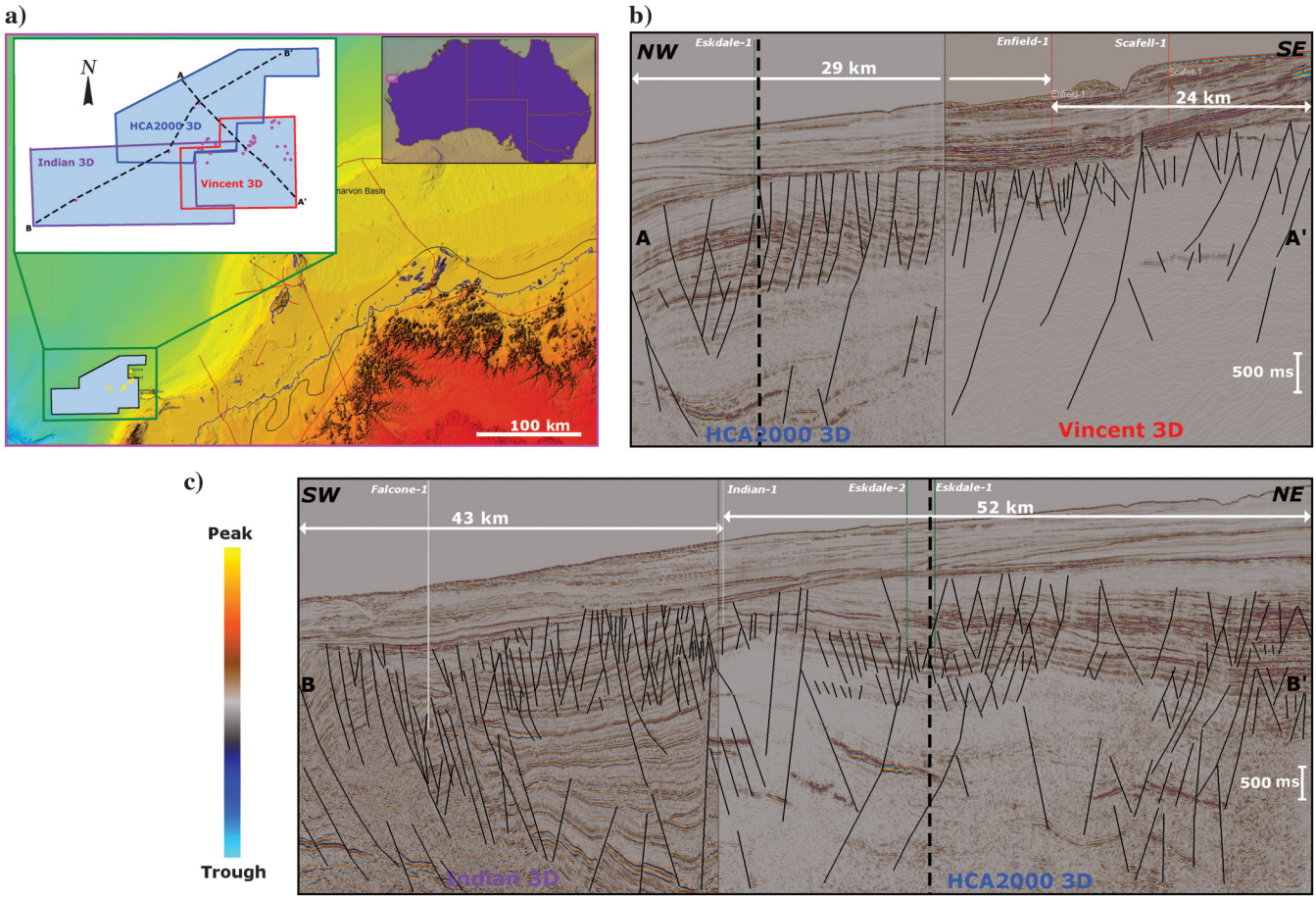

Figure 1. (a) Basemap showing location of Indian, Vincent, and HCA2000A 3D surveys, covering 3500 km^2 of the Exmouth Subbasin, northwestern Australia. Marked on the basemap are two intersecting structurally interpreted arbitrary lines: (b) northwest–southeast line comprising sections of HCA2000A and Vincent surveys and (c) southwest–northeast line comprising sections of Indian and HCA2000A surveys.

northeast–southwest structural trend), to a passive margin carbonate shelf in the Cenozoic (Tindale et al., 1998). The Late Cretaceous to Holocene part of the basin has been filled by a mixed clastic and carbonate succession. Prerift sediments are of Permian and Early-to-Middle Triassic age and are gas-prone, although these were subjected to an earlier Triassic failed rifting episode. The Upper Jurassic Dingo Claystone is the main oil prone source rock across the Exmouth Subbasin. Proven reservoirs occur within the Barrow group and Dupuy sandstone, with the Muderong shale acting as the regional seal (Regional geology of the Northern Carnarvon Basin, Australia 2012, Offshore Petroleum Exploration Acreage release, 2012). Oil was first discovered in 1998 (Vincent-1) and was followed by several additional oil discoveries including Coniston, Laverda, Stybarrow, Ravensworth, and Stickle, establishing the Exmouth Subbasin as a new oil province with a reserve potential of 300 MMbbl. Two new oil projects commenced production in 2010; the Van Gogh oilfield and the Pyrenees project, comprising the Crosby, Ravensworth, and Stickle oilfields (Government of Western Australia, Department of Mines and Petroleum, 2010).

Details of the three seismic surveys used in this study are summarized in Table 1. The data are stacked and migrated time volumes of negative standard polarity (peaks are soft, decreasing impedance events). The setting is shelfal and water depth varies between 90 and 1560 m across the three data sets. All the data sets were acquired through a dual shooting source (flip flop) with receiver spacing of 12.5 m. The spectral content of the three data sets is high, with bandwidth (range) at 50% power of the peak frequency of 59 Hz (15–74 Hz) for Indian 3D, 47 Hz (17–64 Hz) for HCA2000A 3D, and 51 Hz (14–65 Hz) for Vincent 3D. Few processing parameters were supplied with the data, and therefore the effects of the preprocessing sequence and migration are not considered.

Methodology

The workflow applied to each of the Exmouth Subbasin data sets involves several sets of processes which can be categorized into the following stages: data conditioning, structural and fault expression, and stratigraphic expression. Each processing stage contains numerous substeps whereby individual attributes are computed or derived. It is normal for these processing sequences to involve multiple steps where the output of a given process is used as input to, or combined with, another process. A processing flowchart summarizing the substeps is given in Figure 2. The attributes selected for use in this study are not definitive, as hundreds of different seismic attributes exist, which can highlight or delineate a particular feature through its seismic signature. The attributes used here are chosen satisfy the requirement of rapid basin-scale reconnaissance, and it is possible that other attributes could be equally successful in this remit.

Data conditioning

The initial stage of the workflow is to apply noise cancellation to the seismic data. There are two stages to the noise cancellation applied in series. First is the application of a structurally oriented finite impulse response median hybrid (SO FMH) filter (modified from Astola et al., 1989), primarily to attenuate coherent noise within the data set. Any residual random noise is targeted through iterative application of an edge-adaptive tensor diffusion filter (based on anisotropic diffusion filters described in Perona and Malik, 1987).

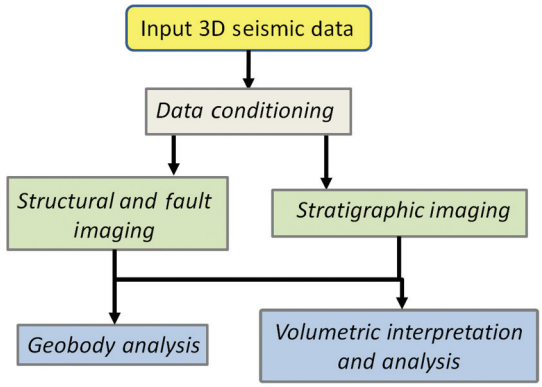

Figure 2. Workflow applied to the processing of the Exmouth Subbasin data sets.

Table 1. Survey details for the three Exmouth Subbasin data sets showing the full survey name, unique survey number (UNO), aerial coverage of live data, acquisition date, survey increments, spheroid, and geographic projection and contractor and client.

Survey Name	UNO	Coverage (km^2)	Completion date:	Postprocessing Sampling interval (increment)			Spheroid/ Projection	Contractor/Client
				IL	XL	t		
Indian 2000 3D MSS	S6200017	1150	31/12/2000	14.1 m (–1)	9.4 m (1)	4 ms	WGS84/50S	Geco Prakla/ Woodside
HCA2000A 3D MSS	S6200029	1000	21/02/2001	28.1 m (1)	12.5 m (1)	4 ms	WGS84/49S	Western Geco/ BHP
Vincent 3D MSS	S6980024	878	06/03/1998	14.1 m (–1)	12.5 m (1)	4 ms	WGS84/49S	PGS/Woodside

The use of structurally oriented adaptive filters is to improve reflector continuity by smoothing along events, while simultaneously identifying and preserving real discontinuities such as stratigraphic terminations and faults.

Moderate sizes and several passes of noise cancellation filters are deemed most appropriate for attenuating coherent and random noise in each of the data sets (SO FMH = 5 to seven voxels; tensor diffusion = 10 Iterations). A moderate noise cancellation is also a practical compromise due to the variable data quality within the large areas processed. An example of original and noise-canceled sections from the HCA2000A seismic survey is shown in Figure 3.

Structural and fault expression

The overall structural framework in the data sets is expressed effectively through the use of dip and azimuth attributes which express the lateral and vertical components of reflector orientation, and their composite which bins and remaps volumetric dip and azimuth into a single volume which can be displayed using a complementary stereographic colormap (Dalley et al., 1989). Dip-azimuth for detailed structural imaging gives best results with a small filter size. This involves computing the dip and azimuth attributes within a 3D filter with lateral size (x/y) in the range of 5–9 voxels (~65–140 m on these data sets) and vertical filter size seven voxels (28 ms on these data sets). The final azimuth output volume is rotated to north to facilitate interpretation between surveys.

There are a multitude of seismic attributes that have been derived to identify edges using seismic data and each is sensitive to faults with different expressions and on different scales. We have opted to consider a range of edge attributes, namely structurally oriented semblance (SOS), tensor, and structurally oriented discontinuity (SOD), and use them in combination.

SOS is a multitrace semblance measure based on the eigenstructure of the covariance matrix formed from traces in the analysis cube (Gersztenkorn and Marfurt, 1999). It is primarily used to identify faults, although when parameterized at a small scale it also gives a good response to stratigraphic discontinuities (Marfurt et al., 1999) and as an edge attribute, is particularly sensitive to faults and edges that are expressed as variations in-phase. The use of the gradient structural tensor to compute edges is well established (in image processing Harris and Stevens [1988]; for seismic fault analysis, see Bakker, 2002). Here, we use a gradient structural tensor-based measurement as a volumetric edge attribute and because of its sensitivity to strong variation in the structural tensor, it is sensitive to edges that are expressed as a change in amplitude. SOD is an ffA proprietary attribute that we use as an intermediate between SOS and the tensor-based edge measurement. It is sensitive to edges that are expressed as variations in amplitude and phase.

Due to the variability in sensitivity of each edge attribute at detecting discontinuities with different physical expressions within the seismic data (amplitude or phase variability or both) it is more effective to create a composite fault attribute from the individual edge volumes, than considering a single fault attribute alone. Using a multiattribute approach for fault definition is well documented (Purves and Basford, 2011; Iacopini et al., 2012), and it allows us to obtain a fault response that combines the best aspects of each of the component edge volumes. Two methods were used to create the composite fault response:

1) A multiattribute method whereby the individual edge attributes are color blended using a cyan-magenta-yellow (CMY) color scheme. Each attribute is assigned a separate color channel and in the composite image, where a single attribute dominates, so too will the associated color. A high response in all three attributes, results in a blend of the three component colors, which in CMY colorspace is black. Therefore, high probability of faulting, expressed as high values in all three attributes, is defined by dark colors or black in the composite CMY blend. The CMY blend here is composed of the individual fault attributes; SOS is represented as cyan, tensor as magenta, and SOD as yellow. The input attributes are automatically normalized to a common value range during the blend optimization stage. Color perception is crucial in many aspects of interpretation (Froner et al., 2013) and by varying the color-attribute combinations in the blend, different features appear with more or less distinction. Similarly varying the input attribute will give a different color response, and thus a "Dip-SO semblance-tensor" CMY color blend is also used to simultaneously image

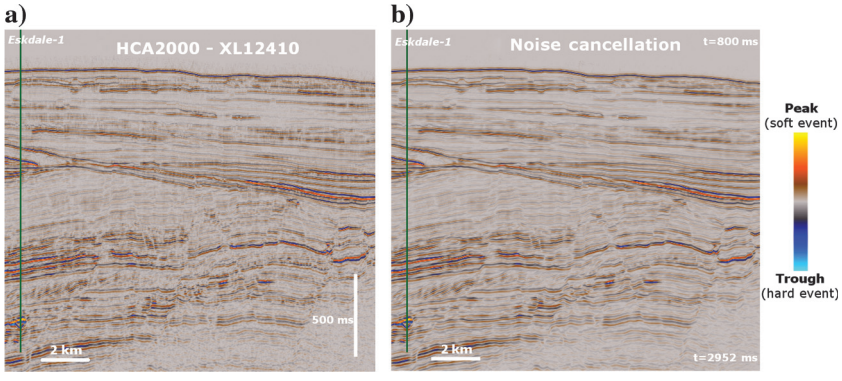

Figure 3. Result of noise cancellation on a sample section of HCA2000A at crossline 12,410, intersecting the gas producing Eskdale-1 well; (a) the original data shows greater discontinuity along reflectors caused by coherent and random noise, whereas (b) the noise-cancelled data has greater continuity along reflectors whilst preserving subtle details.

faults and reflector deformation at multiple levels in the three data sets.

2) An alternative composite fault workflow is to compute a more traditional single-attribute response, which is composed of a stacked average of the different edge attributes. To create this composite, the attributes are summed using the same normalization factors that were used for the CMY blend as attribute scalars, thereby making sure the components are of common value range and a single attribute with higher global values does not dominate the stack. The individual attributes were enhanced before stacking so that the final composite has greater continuity along fault planes. Enhancement is carried out via a Gaussian smoothing operator, which is implemented to improve continuity of faults and reduce the nonfault related clutter within the fault attribute (Nicolescu and Medioni, 2003). The enhanced and stacked fault attribute is used as the input to fault detection utilizing a ridge detection operator (Gauch and Pizer, 1993). The value mapped on to the detected lineations is directly related to input edge attribute value and thus represents the likelihood of the fault being present within the data. The lateral orientation of the fault detect lineation is computed as a fault trend volume, where the attribute value varies with fault strike. This gives an indication of the families of faults present based on their orientation, which appear as different colors and which generally relate to different structural episodes. The fault trend attribute, as with reflector azimuth attribute, is rotated to geographic north to allow comparison between data sets.

Stratigraphic expression

The stratigraphic expression section of the workflow involves several trace and stratigraphic attributes, and has some overlap with the structural expression workflow. This overlap between structural and stratigraphic imaging also reflects the relationship between the tectonic and stratigraphic evolution of the Exmouth Subbasin. For instance, edge attributes, usually used for imaging faults, also have sensitivity at highlighting stratigraphic edges such as channel boundaries, and stratigraphic imaging techniques can be applied to understand structures, such as the relative offset of fault blocks.

Many of the stratigraphic attributes give nonunique responses and are best interpreted within the framework of a depositional model. Such combination with *a priori* knowledge of type and geometry of sedimentary systems will help to identify and distinguish features of interest based on size, shape, and attribute value (which is usually visualized as color). When properly interpreted with background knowledge, analogs, and models, stratigraphic attributes provide a powerful tool for rapidly exploring large extents of seismic data. A brief description of the stratigraphic attributes that have been used to reconnoiter these three large data sets and also to explore reservoir level features in detail is presented.

The envelope complex trace attribute (Taner et al., 1979) is used as a measure of reflection strength and it is sensitive to high acoustic impedance contrasts within seismic data. Frequency decomposition is a method of extracting band-limited versions of the seismic data, by convolving a wavelet of known central frequency and bandwidth with each seismic trace. Gabor wavelets are used as the decomposition wavelets due to their close approximation to a seismic pulse (Morlet et al., 1982). The decomposition frequencies and bandwidths are chosen to reflect the spectral content of the seismic data and also to have sensitivity to particular features of interest through their inherent tuning properties (Partyka et al., 1999). A series of three band-pass magnitude volumes were produced for each data set, with overlapping bandwidth. A Uniform Constant Q decomposition method was employed, whereby the bandwidth increases with frequency to give optimal vertical resolution. The three frequency-magnitude volumes were then color blended using a red-green-blue (RGB) color blend, where each band is represented using an individual color (Henderson et al., 2007). In the resulting blend, where one frequency band dominates, so does that color; where there is an equal and high response from all three banfds, the blend will appear white due to the equal combination of red, green, and blue; and where there is an uneven mix of the band-limited responses, there is an associated blend of colors. The result is an RGB blend that is highly sensitive to changes in thickness and acoustic properties, which are expressed as distinct interference patterns of different colors (McArdle and Ackers, 2012). Displaying such subtle variations in geometry and material properties as chromatic variations enables the interpreter to delineate features with a far greater degree of certainty (Froner et al., 2013).

The bedform attribute provides a simplification of the seismic trace, such that the each peak and trough of the waveform is collapsed to two-voxels and when applied over several traces it results in a series of peak and trough lineations. Additionally, doublets (unresolved events which approach maxima or minima without zero crossing) are distinguished as a different color. The bedform attribute provides a simplification of the seismic reflectivity, independent of amplitude, and is thus particularly suitable for seismic stratigraphic interpretation. In this study, we only consider the peak and peak-doublet bedform lineations, to produce a further simplified and less cluttered attribute image. This is necessary due to the high frequencies in the seismic data (>50 Hz) and resulting closely spaced events.

The operation of terracing involves creating a square/blocky model of the trace waveform, with events distinguished by zero crossing. The blocky terrace model is then populated with a secondary

attribute, in this case either event thickness or amplitude. Terracing is an excellent tool for thin bed analysis and the primary use here, in conjunction with horizon constraint, is to examine reservoir scale tuning properties.

Application of the attributes to basin scale reconnaissance

Structural and fault imaging of Jurassic-Cretaceous units of the Exmouth Subbasin

Figure 4 shows examples of the application of various structural attributes to the three data sets. Although the primary aim of this structural imaging is to gain a better understanding of faults and large scale structures within the basin, simple structural attributes can be used to image structures on a variety of scales. For instance, the dip attribute is shown in Figure 4a with sensitivity to stratigraphic elements, in this case the edges of a Tertiary shallow marine carbonate platform that occurs striking northeast–southwest in the HCA2000A survey, yet the same attribute is used to image large-scale structural features, as shown for the rift normal faulting imaged within the Barrow group, 60 ms below the Hauterivian unconformity, at Mardie Greensand level (Figure 4b). The corresponding azimuthal component of reflector orientation (Figure 4c) is also a useful indicator of faulting by showing subtle flexures and major faults as sharp changes in color. The dip and azimuth combination volumes give the overall reflector orientation, with changes in orientation shown as variance in color and sharp discontinuities (high dip terminations) imaged with high color saturation (Figure 4d). Using color to represent structural trends is effective at delineating two major Jurassic-Cretaceous structural components apparent in this final rift phase; northeast–southwest and west-northwest–east-southeast representing conjugate fault orientations. Later analysis of these structural trends shows that, although rifting ceased by the time of deposition of the Valanginian Muderong Shales and Mardie Greensand, many of the faults remained active or were reactivated (Baillie and Jacobson, 1995).

The potential for imaging the Jurassic-Cretaceous rifting using a suite of structural attributes is demonstrated in Figure 4e, which shows the normal faulting at reservoir level around Enfield-1 within the HCA2000A data. Dip and azimuth combination as used in this analysis distinguishes the presence and orientation of major faults as well as changes in the reflector orientation between the more steeply dipping strata within the rotated fault blocks and the overlying deposits with a shallower regional dip. The combined SOS-tensor-SOD edge attribute is successful at picking out the major lineaments, and this is used to create the fault trend volume also shown in Figure 4e. The fault trend mirrors the dominant northeast–southwest trend observed using reflector azimuth (apparent as yellow-green fault lineations in the image), also observable are the minor west-northwest–east-southeast conjugate faults. The geometry of the faults imaged using this derived fault attribute is typical of an extensional setting, and although many of the faults terminate at the Hauterivian unconformity, some extend into the overlying strata, again suggesting postrift activity. Reducing the faults to such lineations increases the speed of interpretation compared to manual interpretation using seismic reflectivity data alone. In addition to conventional structural and fault attributes, stratigraphic imaging techniques can also be applied to understanding tectonism. Alongside the fault-trend and seismic section in Figure 4e is a frequency decomposition RGB color blend, which in vertical section is extremely useful for imaging the faults and the relative offset between key stratigraphic units. Fault expression in RGB blends is good due to the large size of the band-pass filters resulting in vertical averaging of the seismic fault expression, which in turn increases fault continuity albeit with a degree of verticalization. Relative offset between strata is surmised because each layer has its own frequency and amplitude characteristics, determined by acoustic properties and thickness, and therefore will appear as a specific color (McArdle and Ackers, 2012).

In addition to the major rifting, other structural types of faulting are distinguished in the shallower sections. Polygonal faulting is observed, shown in Figure 4f and 4g, within the Indian survey. Although this faulting can be observed using many different attributes, they appear with great clarity within the frequency decomposition RGB blends. However, a composite of edge attributes, in the form of a CMY blend of the SOS (cyan), tensor (magenta), and SOD (yellow) attributes, show the same faults with greater contrast and interpretability (Figure 4f). This polygonal faulting is attributed to postrift compaction and dewatering within the Muderong shale. A second CMY blend comprising dip (cyan), tensor (magenta), and SOS (yellow) is shown in Figure 4h over an east–west section of the HCA2000A survey, giving a large-scale structural overview of the subsurface. Including reflector-dip, alongside edge attributes within the CMY blend enables the relative orientation and inferred deformation of stratigraphic layers associated with faulting to be ascertained, along with areas where there is a high confidence in the presence of faults (dark/black in the blend) or low confidence in the interpretability of the attributes (random noise in the blend).

Imaging subsurface stratigraphic features of the Exmouth Subbasin from seismic attributes

Examples of stratigraphic attributes applied to these data sets are shown in Figure 5, alongside a simplified stratigraphic column of the Exmouth Subbasin to correlate the timing and stratigraphic location of each example with the focus on the Jurassic-Cretaceous sand units with reservoir potential.

A west–east line showing the peak bedform attribute for Vincent puts the sequences into a seismic stratigraphic context (Figure 5a; stratigraphic section

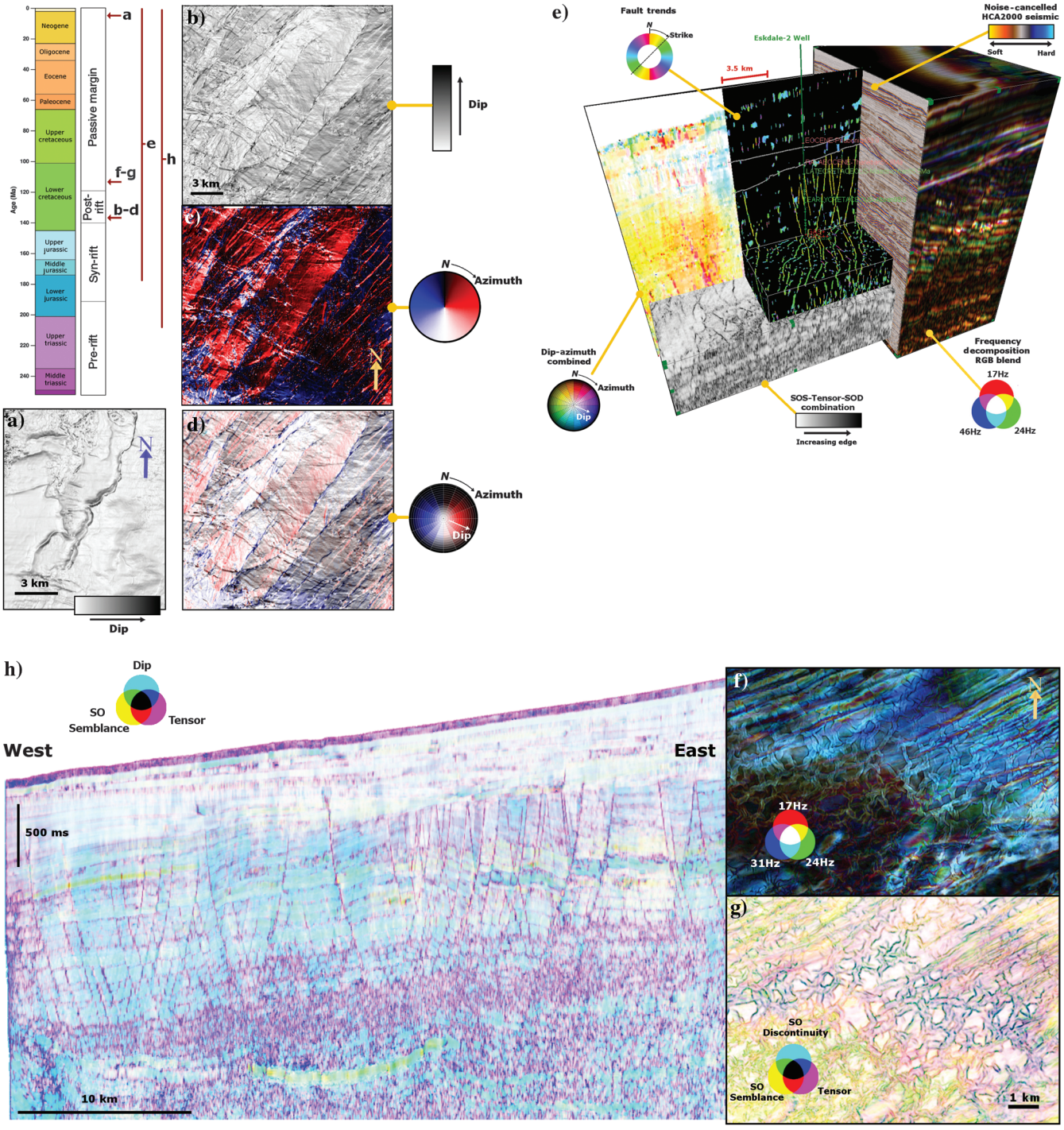

Figure 4. (a-d) Examples of structural and fault attributes applied to the Exmouth Subbasin seismic data to distinguish structural elements. The location relative timing of each subimage in the figure is shown against a timescale with major structural episodes (see main text for full description). (a) The dip attribute showing carbonate platform of the Delambre Fm, observed in the shallow sections of HCA2000A; (b, c, and d) dip, azimuth, and dip azimuth combined, showing normal fault reactivation at Mardie Greensand level, in Vincent 3D. (e) Examples of structural and fault attributes applied to the Exmouth Subbasin seismic data to distinguish structural elements (see main text for full description), (e) structural elements within HCA2000A, imaged using dip-azimuth, composite SOS-tensor-SOD, fault-trends, and frequency decomposition RGB blend. (f, g, and h) Examples of structural and fault attributes applied to the Exmouth Subbasin seismic data to distinguish structural elements (see main text for full description), (f) polygonal faulting due to compaction of early Cretaceous sediments in the postrift phase imaged within the Indian 3D data set using frequency decomposition RGB blend and (g) dip-tensor-SOS CMY blend; (h) dip-tensor-SOS CMY blend at HCA2000A inline 602, giving a broad structural overview of the basin particularly the Jurassic-Cretaceous rifting.

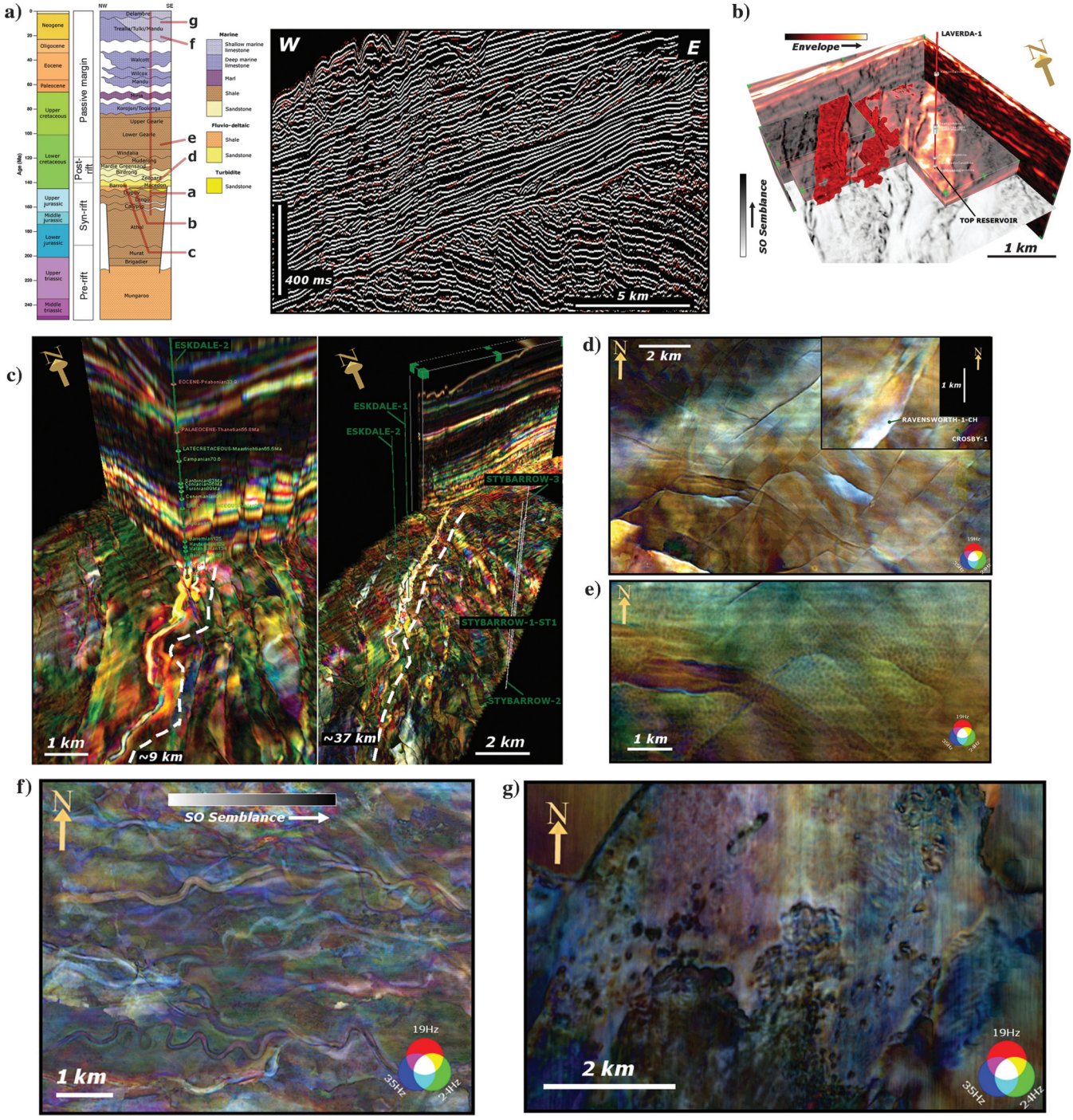

Figure 5. (a) Various depositional elements imaged using stratigraphic imaging techniques and shown at their location within a simplified stratigraphic sequence of the Exmouth Subbasin (see main text for detailed description). Bedform attribute giving a simplified stratigraphic model (Vincent 3D), reflectivity peaks locations are white, unresolved peak doublets are red. (b) Various depositional elements imaged using stratigraphic imaging techniques. Envelope and SO semblance, as slices and combined as an opacity blend, delineating the Macedon turbidite sands intercepted by Laverda-1, and which can be used to create Adaptive Geobodies of the reservoir and neighboring stratal elements (Vincent 3D). (c) Various depositional elements imaged using stratigraphic imaging techniques Barrow group fluvial channel sands intercepted by Eskdale-1 and 2 imaged using RGB blend (HCA2000A 3D). (d and e) Various depositional elements imaged using stratigraphic imaging techniques. (d) Barrow Group sands, showing accumulations of hydrocarbons at sealing faults, apparent as brightening of the RGB blend (Vincent 3D). Inset are images of the same accumulations at Ravensworth-1 and Crosby-1. (e) Leopard-skin mottling occurring in Gearle shales due to compaction and dewatering, RGB blend (Vincent 3D). (f and g) Various depositional elements imaged using stratigraphic imaging techniques. (f) Neogene sinuous fluvio-deltaic channels, RGB-SOS Opacity blend (Vincent 3D). (g) Karstification within the Mandu shallow marine carbonates, RGB blend (Vincent 3D).

modified from BHP Petroleum PTY Ltd., WA-255-P(2) Knott-1 Well Completion Report, Basic Data Volume, April 2005). This highlights prograding clinoforms, channelized deposits, deep marine laminar deposits, and rotated fault blocks. Peaks, shown in white, are easily tracked visually using the bedform attribute and corresponding pinchouts caused by reflector thinning are observed through peak convergence and as doublets, shown in red. The deeper reservoir intervals that have been imaged occur in the Macedon member turbidite sand. An example at well Laverda-1, which is gas-bearing over this interval (Woodside Petroleum Ltd., 2001, Laverda-1, Well Completion Report, Interpretive Data, WA-271-P, Carnarvon Basin), is shown in Figure 5b. A combination of edge (SOS) and infill (envelope) attributes is particularly effective at delineating the reservoir due to its large amplitude anomaly and distinct stratigraphic boundary. Fluvio-deltaic channels of the Barrow group also have proven reservoir potential and an example, with northeast–southwest orientation is illustrated using the 17-24-46-Hz RGB blend derived from the HCA2000A seismic survey (Figure 5c). The Eskdale canyon complex shown in the image is tracked over 37 km. The nature of the channel response varies over this distance; toward the northeast, there are bright homogenous responses, likely of the channel core and at the southwest a more complex and variable response in color and amplitude. It is intercepted by Eskdale-1 and -2, both of which have oil and gas shows (Eskdale-2 has 24.0 m net gas/12.9 m net oil pay; BHP Petroleum PTY Ltd., WA-255-P(2) Eskdale-2 and Eskdale-2/CH1 Well Completion Report, Interpretive Volume, March 2005) and it is highly probable that these hydrocarbon accumulations have resulted in amplitude and frequency variations which are discernible through frequency decomposition and color blending. The variation in color and amplitude in the RGB blend along the length of the Eskdale channel, may reflect changes in thickness and/or facies changes with increased shale content in the more distal deposits. Mapping these changes is very important as it has implications for net to gross, porosity and permeability, thickness prognosis, and ultimately reserve estimates. The Eskdale channel is heavily faulted, and several of these fault segmented channel elements have a similar response in the RGB blend to the reservoirs at Eskdale-1 and -2, indicating that they may have similarities in reservoir properties. Reservoir level of the Barrow group sheet sands is imaged in the RGB blend (Figure 5d), toward the easternmost part of the subbasin. Hydrocarbon deposits are clearly seen as very bright regions of accumulation against sealing faults. This interpretation is confirmed by the inset image which shows similar characteristics in amplitude and frequency at the reservoir level of Ravensworth-1 well, which encountered 42.8 m of net sand pay over the Pyrenees Mbr reservoir interval, with 6.6 m gas-bearing and 36.2 m oil-bearing (BHP Petroleum PTY Ltd., WA-155-P (1) Ravensworth-1/1CH Well Completion Report, Interpretive Volume, May 2004) and Crosby-1 well, which encountered an oil pay of 34 m at the same interval (BHP Petroleum PTY Ltd., WA-12-R Crosby-1 Well Completion Report, Interpretive Volume, June 2004). The use of this method of stratigraphic imaging provides additional means for delineating the lateral extents of these reservoirs and other potential reservoirs. Understanding exactly where these hydrocarbon effects are occurring in the stratigraphic sequence and the relationship they have with the reactivated faulting is important in judging whether there is exploration potential. Where these accumulations occur in Barrow Group sand the permeability of the reservoir permits exploitation. If the faulting extends above the Muderong Shale seal, then accumulations can occur in the Windalia Radiolarite which acts as a thief zone, and which due to its low permeability is deemed of low recoverable potential. Above reservoir level, marine transgression and deeper marine shales of the Gearle Member are encountered. This is imaged in Figure 5e in the 19-24-35-Hz RGB blend and in places this has a distinctive mottling pattern, which, due to the sedimentary environment and lithology, may be attributed to compaction with the underlying Windalia Radiolarite and dewatering. Figure 5f shows typical geometries of fluvio-deltaic channels indicating a coastal depositional environment which occurred in the Neogene, and is imaged using an opacity blend of the 19-24-35-Hz frequency decomposition RGB blend corendered with SO semblance to distinguish channel fill and edges (McArdle et al., 2010). Karstification occurring within shallow marine carbonates of the Mandu formation is shown through RGB blending of 19, 24, and 35 Hz frequency decomposition magnitude volumes derived from the Vincent 3D seismic data (Figure 5g). In this setting, we can correlate the karstification with eustatic sea level curves derived from palynological data collected at nearby wells. These karstified surfaces are easily recognizable evidence of subaerial exposure and dissolution and are of importance to hydrocarbon exploration due to their potential as drilling hazards but also, in the right environment, as reservoirs.

Application of the attributes to detailed analysis

The following section outlines how the seismic attributes generated for basin scale reconnaissance can be used for quantitative analyses and interpretation. First, we look at the variation in the stress field that can be interpreted from the fault trend attribute, and we then examine the use of data-driven, user-guided interpretation for objective reservoir investigation.

Structural expression

A detailed breakdown of the structural trends can be made through rose plot analysis whereby fault trend is plotted as a radial distribution. To determine the variation in structural trend with time, the fault trend volume was cropped between horizons relating to the boundaries of the major structural episodes. The rose

plot is a radial histogram, and 64 radial bins were used, with bins in fault trend data every 5.63°. The length of the radial bar gives the histogram frequency for that binned range. Resulting rose plots for the Vincent 3D survey are shown in Figure 6 and the primary and secondary trends for all three surveys, to the nearest center of bin, are given in Table 2. The dominant trend in the near subsurface is the acquisition direction (east–west) and so that this trend does not dominate and interfere with trends at deeper levels, all fault strike directions between 084° and 096° have been omitted from subsequent analyses as seen in Figure 6. The primary trend is taken to be the fault-trend bin with highest frequency in the rose plot. Also, as an attempt to understand conjugate faulting, the secondary trend is also determined as the second highest frequency bin that occurs in the rose plot (apart from the acquisition direction). There is good agreement between the trends observed in all three surveys. We can compute mean structural-fault orientations for the three surveys for each structural episode. All surveys have an east–west (087°) dominant trend for the near-surface which reflects the acquisition direction. The oldest primary structural trend relates to the Triassic-Jurassic prerift phase and this gives a mean primary (secondary) structural trend of 059° (117°). The subsequent Jurassic-Cretaceous rifting returns a mean primary (secondary) fault trend of 048° (108°) and this northeast–southwest structural trend is well described in literature as relating to the breakup of East Gondwana (Tindale et al., 1998). The next structural episode is the Cretaceous immediate postrift phase which returns a mean primary (secondary) trend of 100° (065°), indicating a change to the stress field. This trend remained stable throughout overlying Palaeogene and Neogene sediments, and these units return a dominant primary (secondary) orientation of 098° (065°).

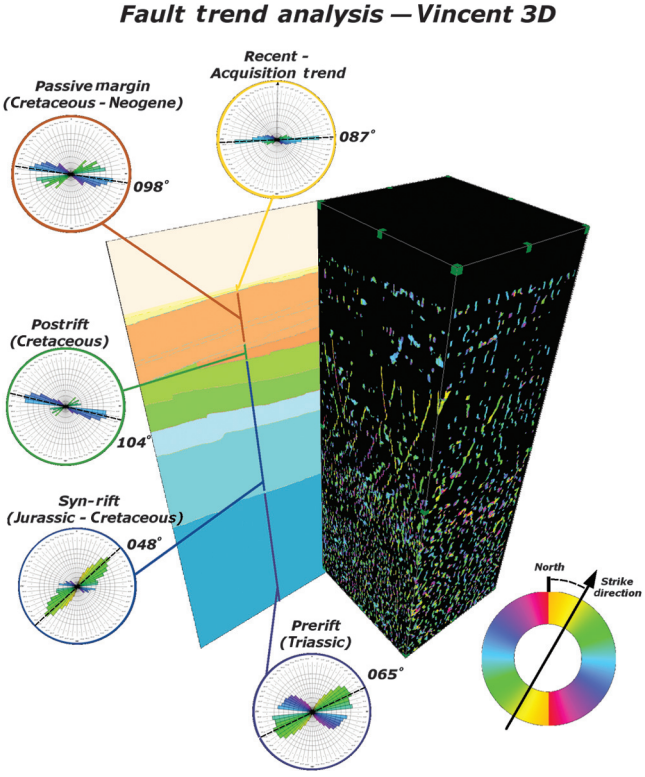

Figure 6. Fault trend rose plots generated at key intervals in the Vincent 3D survey using horizon constraint. The background (acquisition) trend was isolated in the near subsurface and this trend was omitted from the other analyses. The primary dominant trend is given at each level.

The earliest Triassic phase is prerift and the primary and secondary directions at this time are rotated by 10° with respect to the later synrift phase (Triassic to Jurassic; primary trend from 059° to 048°; secondary trend from 117° to 108°). This is interpreted as a rotation of the stress field and the earlier component may represent the trend at the first initiation of rifting that occurred deeper in the section. The secondary trends are more complex, as they are more likely to relate to conjugate faults and overprints, and the primary and secondary Triassic structural trend includes a component from the later Jurassic-Cretaceous rifting. The Jurassic-Cretaceous synrift phase, as Australia and India moved apart, is epitomized by conjugate faulting and the conjugate direction is shown through the mean secondary dominant orientation for the synrift phase

Table 2. Dominant structural-fault trend directions, for the three surveys, ascertained from rose plots from the fault trends volume at different stratigraphic intervals. Mean primary (secondary) fault trends of the three data sets are Prerift, 059° (117°); Syn-rift 048° (108°); Postrift, 100° (065°); and Passive-margin, 098° (065°).

Structural episode	Indian 3D primary (secondary) dominant trend	HCA2000A 3D primary (secondary) dominant trend	Vincent 3D primary (secondary) dominant trend
Recent[3]	087° (–)	087° (–)	087° (–)
Cretaceous — Neogene (Passive Margin)[4]	098° (065°)	098° (065°)	098° (065°)
Cretaceous (postrift)[4]	098° (065°)	104° (065°)	098° (065°)
Jurassic — Cretaceous (synrift)[4]	042° (132°)	048° (076°)	053° (115°)
Triassic — Jurassic (prerift)[4]	048° (132°)	065° (104°)	065° (115°)

[3]Acquisition trend dominates.
[4]Acquisition trend is removed.

as 108°. It is particularly interesting that some of the faults in the postrift phase continue directly from the major rift associated normal faulting, and the fact that the orientation of these faults change from northeast-southwest to east-southeast–west-northwest, indicates that it is likely that the faults were reactivated postrift, rather than staying active. Understanding and analyzing fault reactivation is of high significance to explorationists in the Exmouth Subbasin because these faults can compromise the Muderong Shale regional seal and can be responsible for charge in the overlying low permeability Windalia Radiolarite which acts as a thief zone. The most recent discernible structural trend relates to the time between Cretaceous-Neogene during which the Exmouth Subbasin evolved as a passive margin and the stability of the stress field in this time is demonstrated by consistency in the mean orientation of the structural trends (from Cretaceous to Neogene; primary trend from 100° to 098°; secondary trend is stable at 065°). The fact that the mean primary and secondary orientations have remained the same (to within 2°) since the immediate postrift phase of the Lower Cretaceous is a good indicator that the stress field has not significantly changed within this time.

Stratigraphic expression

Once stratigraphic targets have been identified using these reconnaissance attributes, potential or known reservoirs can be explored in detail. The purpose of extracting localized features can be for prospect generation, or alternatively for attribute calibration, especially if there is existing well control. A technique for exploring these prospects involves creating adaptive geobodies; these are data-driven, user-guided interpretation objects based on a single or multiple attributes. They are user-guided in that the interpreter selects where a geobody should grow using seed points, or even an initial shape, as initialization. The geobody then morphs to fit areas with the same statistical distribution as that about the seed points, although the user maintains control over when to stop deformation or to override it by including manual manipulation of the geobody. This approach is very intuitive, and allows for interpretative expertise and geologic knowledge to be combined with a thoroughly objective data-based delineation. The final stratigraphic example shows geobody analysis carried out at the Laverda-1 reservoir, a faulted Macedon turbidite deposit (Figure 7). The geobodies shown here were created using the envelope attribute to distinguish sand from background shale, and the SOS attribute to delineate the edges and fault bounds. An opacity blend of SOS and envelope is a very effective way of covisualizing this complementary information (Chopra and Marfurt, 2006). Notable in this example are similar faulted turbidite sands, above and to the north–west of the Laverda-1 reservoir, which may also have exploration potential.

As well as treating adaptive geobodies as purely interpretational surfaces, it is possible to use them in conjunction with more conventional volume attributes to discern further information about the stratigraphic feature being investigated. Of critical importance when making a seismic attribute investigation is understanding the tolerance and sensitivity of the seismic data for resolving features, and an example of how a combination of adaptive geobodies and volumetric analysis can be used to investigate the tuning properties for sensitivity analysis is shown in Figure 7 for the Laverda-1 Macedon reservoir. The adaptive geobody surfaces generated using envelope and SOS are first converted to volumes, which in turn are populated with seismic attribute values. For tuning analysis, two geobody cropped volumes are created; these are body volumes which contain absolute values of wavelet amplitude and thickness obtained from the terrace attribute. When amplitude is crossplotted against thickness, a tuning model for the reservoir is realized and this plot defines the limit of seismic resolution due to interference as thin beds converge (Widess, 1973). It is shown here that the tuning point in time for these Macedon sands occurs at 14 ms, which, using an interval velocity of 2.72 kms^{-1} (from the Laverda-1 checkshot at Macedon interval)

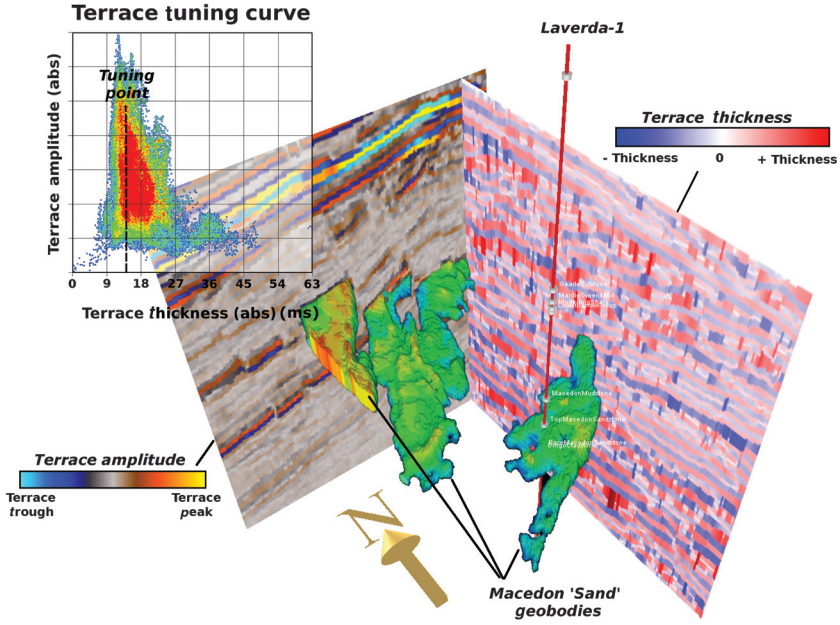

Figure 7. Tuning analysis based on adaptive geobodies of Laverda-1 turbidite sands. The adaptive geobodies are converted to volumes which are populated with absolute values of Terrace amplitude and thickness. The tuning curve is created by crossplotting these thickness and amplitude values. The peak in amplitude occurs where there is maximum constructive interference as thinning events converge.

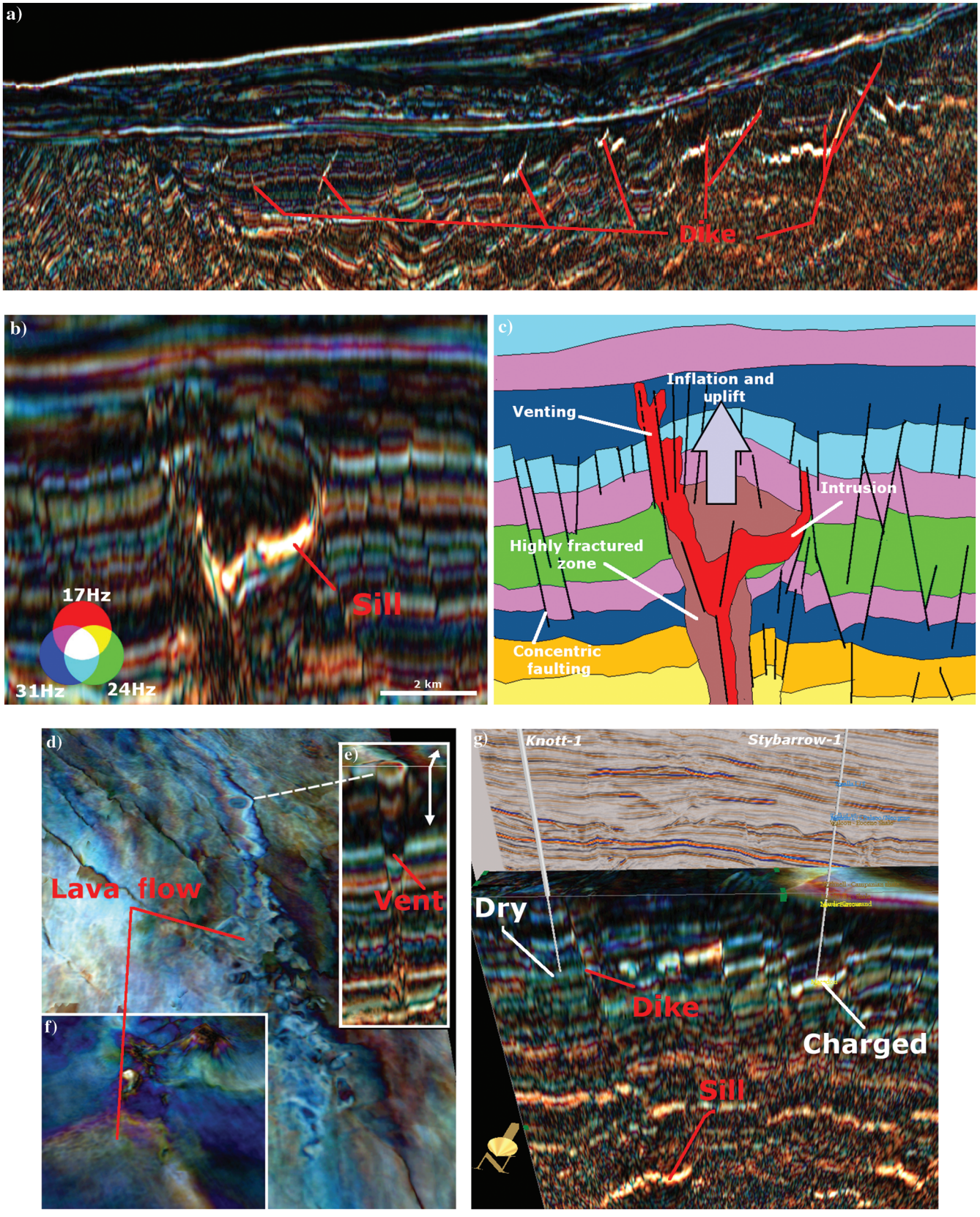

Figure 8. Various igneous elements of the Exmouth Subbasin imaged through frequency decomposition RGB blending: (a) Synrift dikes exploiting normal faults (Indian); (b and c) Sill intrusion and associated structural deformations (Indian); (d) lava flow at Muderong shale occurring at the final stages of rifting (Indian); (e) vent feeding extrusion (Indian); (f) volcanic extrusion (Vincent); and (f) dike fed by deeper sill separates Knott-1 and Stybarrow-1 wells, which are dry and charged, respectively. Here, the dike might be acting as a baffle to hydrocarbon migration and be responsible for the Knott-1 dry well (Indian).

can be converted to a tuning thickness of 38 m in depth. The tuning point is a very important measurement of seismic sensitivity for below this point, events cannot be fully resolved. Performing tuning analyses on a reservoir scale, using geobodies as constraints may be more preferable than doing similar operations across a larger volume or horizon because any variations in resolution due to attenuation or other dispersive effects will be minimized and the overall results more focused.

Another byproduct of understanding the tuning thickness is its relationship with predominant frequency (Kallweit and Woods, 1982). Tuning thickness for these Macedon sands relates to a predominant frequency of 28 Hz. Knowledge of the sensitivities in the frequency domain enables the frequency decomposition parameters to be refined to match the localized reservoir thresholds and can aid understanding of the decomposition responses.

Igneous history of Exmouth Subbasin from seismic attributes

The magmatic history of the Exmouth Subbasin in relation to faulting and inferred from seismic data has already been explored (Magee et al., 2013). However, in the course of this study, intrusive episodes and volcanism have been imaged in notable detail. Igneous systems are of interest to hydrocarbon exploration in several ways (Holford et al., 2012). Primarily dense igneous rock provide drilling hazards that are to be avoided, but also intrusive rocks can influence hydrocarbon migration pathways by acting as baffles; they can provide reservoir seals influencing compartmentalization and create structural closures through inflation and uplift. Reworked volcanic material may act as a sediment source, and porous igneous rocks, such as pyroclastic deposits, can also have reservoir potential in their own right. Magmatic-induced heating of the subsurface can also affect hydrocarbon maturation in a positive or negative way depending on the source rock and temperatures involved. Many classic saucer-shaped sills have been emplaced throughout the Exmouth Subbasin. They are thought to be synrift, from Late Jurassic to Early Cretaceous in age (Mihut and Muller, 1998), and are visible in the seismic as high-amplitude anomalies through their distinctive geometry and localization. They are fed by a network of dikes that have exploited the rift faulting as planes of weakness and they are seen to vent (Figure 8).

Figure 8 illustrates how the igneous system is inherently linked to the Exmouth Subbasin petroleum system. Dikes are seen to intrude large extents of the rifts, and these were synchronous with the rifting episode (Figure 8a). On a more detailed level, we can see the effect of intrusion on the surrounding stratigraphy (Figure 8b), where the emplacement of a sill resulted in deformation. The response in the RGB blend is chaotic in the baked and fractured zone immediately surrounding the intrusion. Above the intrusion, there is a degree of uplift and in the surrounding region concentric faulting occurs. These features are shown schematically in Figure 8c. The igneous systems are not limited to the intrusive. Figure 8d shows lava flows at the Muderong level, fed by a vent shown in Figure 8e. More paleovolcanic features are shown in Figure 8f at Muderong level and the fact that these occur above the major rift faulting suggests that the igneous system was still active in the early postrift phase. The potential implications for the hydrocarbon system is shown in Figure 8g, where the Knott-1 well (dry hole; BHP Petroleum PTY Ltd., WA-255-P(2) Knott- 1 Well Completion Report, Basic Data Volume, April 2005) and Stybarrow-1 (charged; BHP Petroleum PTY Ltd., WA-255-P(2) Stybarrow-1/1CH Well Completion Report, Interpretive Volume, February 2004) wells are separated by a dike exploiting a normal fault. It is possible that this dike acts as a baffle to hydrocarbon migration and is responsible for the Knott-1 well being dry at the Macedon Sand reservoir level.

Conclusions

The aim of this study was to outline the use of multiattribute workflows for basin scale exploration and target level interpretration, to determine the subsurface geologic expression of the Exmouth Subbasin. We have shown how seismic attributes allow rapid reconnaissance of large acreage which can be rapidly focused to reservoir scale for attribute calibration and prospect generation. We have demonstrated that various fault and structural attributes can be employed to aid interpretation of major structural features, from simple attributes such as dip and azimuth, and SO semblance edge attributes, to more complex combinations, blends, and derivatives. Using multiattribute combinations is an effective way of covisualizing several attributes that image a geologic system in different ways, giving a more complete description where a single attribute would only give a partial solution.

The use of seismic attributes in reconnoitering the Exmouth Subbasin is shown to highlight a wide range of structural and stratigraphic features. The major rift event is imaged through combination and color blending of edge attributes and these are used to produce fault trend lineations that are further analyzed at discrete stratigraphic intervals. The fault trend analysis shows that there is a distinct change in trend between the synrift and postrift settings; continuation of individual faults across this boundary with different orientations suggest fault reactivation, which is important when evaluating the integrity of the regional Muderong seal. Detailed analysis of the derivative attributes, such as the fault trend volume enables robust structural orientations to be rapidly obtained with minimal manual interpretation. A comparison of attributes and structural trends obtained between the three surveys shows a high degree of repeatability and it can be inferred that the same techniques can be applied to data sets from different geologic settings and of different quality to meet the same reconnaissance objectives.

Stratigraphic imaging at a basin-scale reconnaissance level was conducted through trace attributes namely envelope and bedform analysis and through frequency decomposition and RGB blending. This was extremely useful in distinguishing various depositional elements related to the hydrocarbon system and can be used to quickly refine conceptual models of deposition. By comparing stratigraphic and structural attributes, a tectonostratigraphic reconstruction can be visualized for the different intervals. The inherent connection between structural episodes and related depositional environments is mirrored in how structural and stratigraphic attributes complement each other visually, through overlays and blending, and computationally as a combined input to other processes. For reservoir scale-focused interpretation, it is shown that adaptive geobodies can be used to interpret a geologic element in a data-driven but user-guided manner. This allows rapid and objective play concept and sensitivity testing of the target. Once a geobody or collection of geobodies has been interpreted, detailed tuning analyses can be made by combining the adaptive geobodies volumetrically with terrace attributes. Performing reservoir-scale tuning analyses is important for understanding the fundamental seismic resolution thresholds and the related frequency ranges, which in turn can be used to refine frequency decomposition parameterization and interpretation of RGB blends.

Stratigraphically, many different depositional elements are observed in detail through frequency decomposition and color blending. Specifically, the faulted Cretaceous Barrow Group, fluvio-deltaic, turbiditic, and laminar sands are imaged at basin to reservoir scale. The interplay between structure and stratigraphy is primarily observed through rifting and offset of these channelized and sheet-sand elements, and this is important to understand when reconstructing the depositional environment. The magmatic history is inherently linked to rift tectonism and understanding the plumbing of the igneous system is necessary for evaluating the impact on the hydrocarbon system, and so that drilling hazards and potential baffles can be avoided.

Acknowledgments

We acknowledge Geoscience Australia for the release of the seismic and well data used in this study through the 2010 Acreage release, ffA staff for discussions and the reviewers, Abdullatif Al-Shuhail, Arthur Barnes, and Dengliang Gao for critical review of this paper.

References

Astola, J., P. Heinonen, and Y. Neuvo, 1989, Linear median hybrid filters: IEEE Transactions on Circuits and Systems, **36**, 1430–1438.

Baillie, P. W., and E. Jacobson, 1995, Structural evolution of the Carnarvon Terrace, Western Australia: APPEA Journal, **35**, 321–332.

Bakker, P., 2002, Image structure analysis for seismic interpretation: Ph.D. thesis, Technische Universiteit Delft, 32–34, 100.

Chopra, S., and K. J. Marfurt, 2006, Seismic attributes — A historical perspective: Geophysics, **70**, no. 5, 3SO–28SO, doi: 10.1190/1.2098670.

Chopra, S., and K. J. Marfurt, 2010, Integration of coherence and volumetric curvatures images: The Leading Edge, **29**, 1092–1107.

Dalley, R. M., E. C. A. Gevers, G. M. Stampfli, D. J. Davies, C. N. Gastaldi, P. A. Ruijtenberg, and G. J. O. Vermeer, 1989, Dip and azimuth displays for 3D seismic interpretation: First Break, **7**, 86–95.

Dutzer, J. F., H. Basford, and S. Purves, 2010, Investigating fault sealing potential through fault relative volume analysis, *in* B.A. Vining, and S.C. Pickering, eds., Petroleum geology: From mature basins to new frontiers: Proceedings of the 7th Petroleum Geology Conference.

Froner, B., S. J. Purves, J. Lowell, and J. Henderson, 2013, Perception of visual information: The role of color in seismic interpretation: First Break, **31**, 29–34.

Gao, D., 2013, Integrating 3D seismic curvature and curvature gradient attributes for fracture characterization: Methodologies and interpretational implications: Geophysics, **78**, no. 2, O21–O31, doi: 10.1190/geo2012-01090.1.

Gauch, J. M., and S. M. Pizer, 1993, Multiresolution analysis of ridges and valleys in grey-scale images: IEEE Transactions on Pattern Analysis and Machine Intelligence, **15**, 635–646.

Gersztenkorn, A., and K. J. Marfurt, 1999, Eigenstructure-based coherence computations as an aid to 3-D structural and stratigraphic mapping: Geophysics, **64**, 1468–1479, doi: 10.1190/1.1444651.

Harris, C., and M. Stephens, 1988, A combined corner and edge detector: Proceedings of the 4th ALVEY Vision Conference, 147–151.

Henderson, J., S. J. Purves, and C. Leppard, 2007, Automated delineation of geological elements from 3D seismic data through analysis of multichannel, volumetric spectral decomposition data: First Break, **25**, 87–93.

Holford, S. P., N. Schofield, J. D. MacDonald, I. R. Duddy, and P. F. Green, 2012, Seismic analysis of igneous systems in sedimentary basins and their impacts on hydrocarbon prospectivity: Examples from the Southern Australian margin: APPEA Journal, **52**, 229–252.

Iacopini, D., and R. W. H. Butler, 2011, Imaging deformation in submarine thrust belts using seismic attributes: Earth and Planetary Science Letters, **302**, 414–422.

Iacopini, D., R. W. H. Butler, and S. J. Purves, 2012, Seismic imaging of thrust faults and structural damage: A visualization workflow for deepwater thrust belts: First Break, **5**, 39–46.

Kallweit, R. S., and L. C. Wood, 1982, The limits of resolution of zero-phase wavelets: Geophysics, **47**, 1035–1046, doi: 10.1190/1.1441367.

Magee, C., C. A. L. Jackson, and N. Schofield, 2013, The influence of normal fault geometry on igneous sill emplacement and morphology: Geology, **41**, 407–410.
Marfurt, K. J., V. Sudhakar, A. Gersztenkorn, K. D. Crawford, and S. E. Nissen, 1999, Coherency calculations in the presence of structural dip: Geophysics, **64**, 104–111, doi: 10.1190/1.1444508.
McArdle, N. J., and M. A. Ackers, 2012, Understanding seismic thin-bed responses using frequency decomposition and RGB blending: First Break, **30**, 57–65.
McArdle, N. J., T. Kristensen, J. Lowell, H. Basford, D. Norton, and S. J. Purves, 2010, Spits, channels and beaches: Advanced imaging and delineation of Jurassic and Triassic stratigraphic targets: PETEX, Extended Abstracts.
Mihut, D., and R. D. Müller, 1998, Volcanic margin formation and Mesozoic rift propagators in the Cuvier Abyssal Plain off Western Australia: Journal of Geophysical Research, **103**, 27135–27149.
Morlet, J., G. Arens, E. Fourgeau, and D. Giard, 1982, Wave propagation and sampling theory — Part I: Complex signal and scattering in multilayered media: Geophysics, **47**, 203–221, doi: 10.1190/1.1441328.
Nicolescu, M., and G. Medioni, 2003, Motion segmentation with accurate boundaries — A tensor voting approach: Proceedings, IEEE Computer Vision and Pattern Recognition, **1**, 382–389.
Partyka, G., J. Gridley, and J. Lopez, 1999, Interpretational applications of spectral decomposition in reservoir characterization: The Leading Edge, **18**, 353–360.
Perona, P., and J. Malik, 1987, Scale space and edge detection using anisotropic diffusion: Proceedings, IEEE Computer Society Workshop, Computer Vision, 16–27.
Purves, S., and H. Basford, 2011, Visualizing geological structure through subtractive color blending: *in* K.J. Marfurt, D. Gao, A. Barnes, S. Chopra, A. Corrao, B. Hart, H. James, J. Pacht, and N. C. Rosen, eds., Attributes: New views on seismic imaging — Their use in exploration and production: 31st Annual Gulf Coast Section SEPM Foundation Bob F. Perkins Research Conference.
Taner, M. T., F. Koehler, and R. E. Sheriff, 1979, Complex seismic trace analysis: Geophysics, **44**, 1041–1063, doi: 10.1190/1.1440994.
Taner, M. T., and R. E. Sheriff, 1977, Application of amplitude, frequency and other attributes to stratigraphic and hydrocarbon determination: *in* C. E. Payton, ed., Seismic stratigraphy: Applications to hydrocarbon exploration: AAPG Memoir **26**, 301–327.
Tindale, K., N. Newell, J. Keall, and N. Smith, 1998, Structural evolution and charge history of the Exmouth Sub-basin, northern Carnarvon Basin, Western Australia: *in* P. G. Purcell, and R. R. Purcell, eds., The sedimentary basins of Western Australia 2: Proceedings of Petroleum Exploration, Society of Australia Symposium, 447–472.
Widess, M. B., 1973, How thin is a thin bed?: Geophysics, **38**, 1176–1180, doi: 10.1190/1.1440403.

Nick McArdle received a B.S. and Ph.D. in geophysics from the University of Liverpool. He works as a principal geophysicist at ffA in Aberdeen, where his primary responsibilities are workflow development and consultancy related to seismic imaging and attribute analysis. His research interests include frequency-related phenomena and interference, AVO classification, and technological advancements in interpretation software.

David Iacopini graduated with a degree in geology and then received a Ph.D. (2002) in earth science from the University of Pisa, working on field structural geology and tectonophysics. He is currently a lecturer in geophysics and structural geology at the Geology and Petroleum Geology Department, University of Aberdeen (UK). Before obtaining that position, he worked as a research assistant in Pisa and Aberdeen, focusing in structural field geology (Sardinia and Himalayan basement), signal processing, and deep water seismic interpretation. His main research interests include quantitative seismic interpretation, fault seismic image processing, and rock deformation analysis at various scales.

Moji KunleDare received B.S. and M.S. degrees from Obafemi Awolowo University, Ile-Ife, Nigeria, and a Ph.D. from the University of Missouri-Rolla (now Missouri University of Science and Technology), USA. She is a senior project geoscientist at ffA, Aberdeen, UK, and was an exploration geologist at ConocoPhillips, Lagos, Nigeria. Her research interests include clastic sedimentology, depositional systems analysis, seismic geomorphology, and seismic attribute analysis.

Gaynor Paton has been part of the geosciences services group with ffA since 2001 and has played a key role in the development of the software and services provided by ffA. She has been involved in attribute analysis and processing on more than 200 different data sets from around the world including Australia, Middle East, North Sea, Gulf of Mexico, onshore USA, and offshore Brazil. These data encompass clastic, carbonate, salt, and shale environments using a variety of source data including reflectivity, acoustic impedance, 4D, multiazimuth, angle stacks, and inversion volumes.